
Accurate Computation of Transfer Maps for Realistic Beamline Elements from Surface Data

Chad Mitchell

Naval Research Laboratory, Washington, DC

Alex Dragt

University of Maryland, College Park, MD

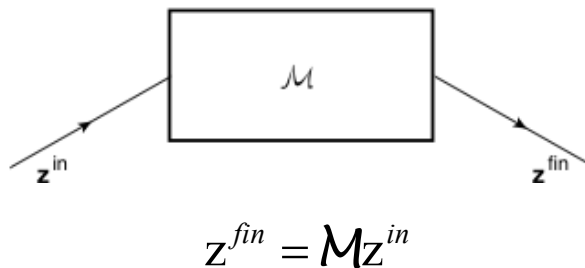


Abstract Summary

- New methods have been found that make it possible, for the first time, to compute accurate high-order transfer maps for realistic beam-line elements to be used in charged-particle optics codes.
- Such methods use 3-d field data, provided on a grid by finite element modeling, to incorporate fringe field effects and nonlinear multipoles into a map description of beam dynamics.
- Once accurate transfer maps have been found for individual beam-line elements, one can determine all single-particle properties of the machine: dynamic aperture, tunes, chromaticities, anharmonicities, linear and nonlinear lattice functions, etc.
- Key is the use of surface data to compute interior data. Surface must enclose design trajectory and lie within all iron or other sources.

Review of map methods

Given the phase space coordinates $\mathbf{z} = (q_1, p_1, q_2, p_2, q_3, p_3)$, we represent the dynamics of a single particle in each beamline element as a mapping:



where \mathbf{z}^{in} and \mathbf{z}^{fin} are the initial coordinates at entry and final coordinates at exit, respectively.

Maps for adjacent beamline elements may be composed (concatenated) to obtain a single map for one full pass through the machine.

Maps resulting from Hamiltonian motion are *symplectic*. The Jacobian matrix

$$M_{jk} = \frac{\partial \mathbf{z}_j^{fin}}{\partial \mathbf{z}_k^{in}}$$

must satisfy

$$M^T J M = J \quad \text{where}$$

$$J = \begin{pmatrix} 0 & 1 & 0 & 0 & 0 & 0 \\ -1 & 0 & 0 & 0 & 0 & 0 \\ 0 & 0 & 0 & 1 & 0 & 0 \\ 0 & 0 & -1 & 0 & 0 & 0 \\ 0 & 0 & 0 & 0 & 0 & 1 \\ 0 & 0 & 0 & 0 & -1 & 0 \end{pmatrix}$$

Given an analytic function f , define a corresponding Lie operator $:f:$ which acts on analytic functions g such that $:f:g = [f, g]$

where

$$[f, g] = \sum_{j=1}^3 \left(\frac{\partial f}{\partial q_j} \frac{\partial g}{\partial p_j} - \frac{\partial g}{\partial q_j} \frac{\partial f}{\partial p_j} \right) \quad \text{Poisson bracket}$$

Similarly, the Lie transformation generated by f is defined by the series

$$\exp(:f:) = \sum_{n=0}^{\infty} \frac{1}{n!} :f:^n$$

Any analytic symplectic map which also maps the origin into itself can then be written

$$\mathcal{M} = \mathcal{R}_2 e^{:f_3:} e^{:f_4:} e^{:f_5:} e^{:f_6:} \dots$$

where \mathcal{R}_2 is the linear part of the map, represented by a matrix R_2 , and each f_m is a homogeneous polynomial of degree m .

Requires expansion about the design orbit $x^d(z)$, $p_x^d(z)$, $y^d(z)$, $p_y^d(z)$ etc. through the beamline element:

$$K = \sum_{s=1}^S h_s(z) K_s(\delta x, \delta p_x, \delta y, \delta p_y, \delta \tau, \delta p_\tau)$$

terms of degree 1 – design orbit
 terms of degree 2 – R_2
 terms of degree > 2 – f_m

Computing Accurate Maps

Suppose $\mathbf{E} = 0$. To obtain the $h_s(z)$, we need expressions of the form:

$$A_w(x, y, z) = \sum_{l=1}^L a_l^w(z) P_l(\delta x, \delta y) \quad \text{with} \quad w = x, y, z$$

Field data may be available on some 3-d mesh

- measured data (3d magnetic sensors)
- electromagnetic field solvers (eg., finite-element codes)

Numerical differentiation is unreliable for high-order $a_l^w(z)$ due to amplification of noise.

Noise spectrum \sim flat to $k = \pi/h$

Introduces weight to high spatial frequencies not present in true field B_y

$$\frac{\partial^n B_y}{\partial z^n} = F^{-1}[(ik)^n F[B_y]] \quad \text{where} \quad F[B_y] = \frac{1}{\sqrt{2\pi}} \int_{-\infty}^{\infty} e^{ikz} B_y(x, y, z) dz$$

accentuates large spatial frequencies

Surface Fitting

- Fit measured/numerical field data to the boundary surface of a volume containing the design trajectory and excluding all iron or other sources (eg., a long “cylinder” in z with uniform cross-section).
- Interpolate inward using Maxwell’s equations. In a source-free region, solutions are smooth (analytic) functions.
- Obtain an analytic representation of the interior vector potential A and its Taylor coefficients $a_w^l(z)$ in terms of surface data alone.
- Highly accurate and robust against numerical errors. Errors are damped as one moves away from the surface into the interior.

error appearing in derivative of order m $\leq \left(\frac{3m}{d}\right)^m \max_s |\delta B|$ d - distance of closest approach to surface

Advantages of Surface Fitting

- Maxwell equations are exactly satisfied.
- Error is globally controlled. The error must take all extrema on the boundary, where we have done a controlled fit.
- Careful benchmarking against analytic results for arrays of magnetic monopoles.
- Surface integration is *smoothing*. (High frequency errors are preferentially damped, improving accuracy in high-order derivatives.) Insensitivity to noise improves with increased distance from the surface.

For example, in a magnetic monopole doublet test case, adding a 1% surface noise produced only a 0.01% change in the computed transfer map.

Accurate transfer maps can now be computed for realistic beamline elements of any machine, e.g. the ILC damping rings, using surface methods:

- Solenoids and multipoles -- circular cylinder (M. Venturini)
- RF cavities -- circular cylinder (D. Abell)
- Wiggler magnets -- elliptical / rectangular / circular cylinder (C. Mitchell)
- Bending dipoles -- bent box / bent cylinder (C. Mitchell, P. Walstrom)

use known Green's function

use new geometry-independent integration kernels

Consider first the elliptical cylinder.

Fitting ILC Wiggler Data Using Elliptical Cylinder

- Data on regular Cartesian grid

4.8cm in x, $dx=0.4\text{cm}$

2.6cm in y, $dy=0.2\text{cm}$

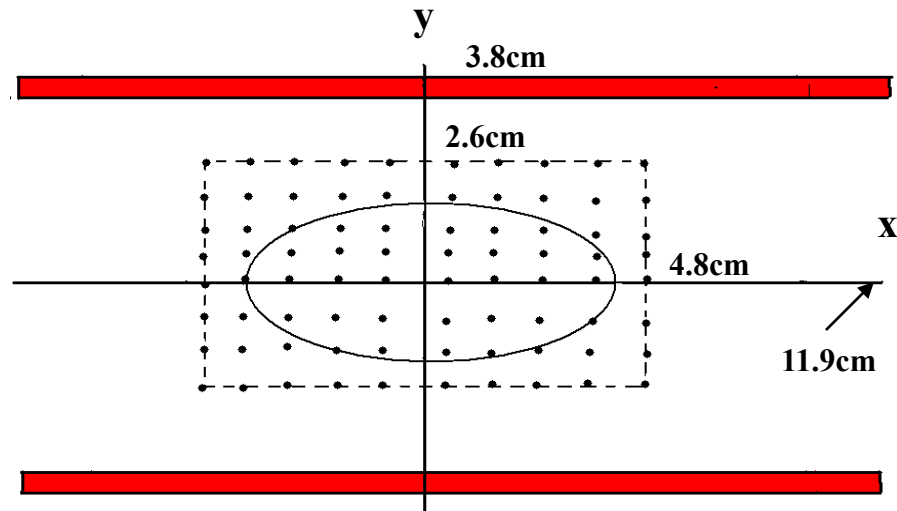
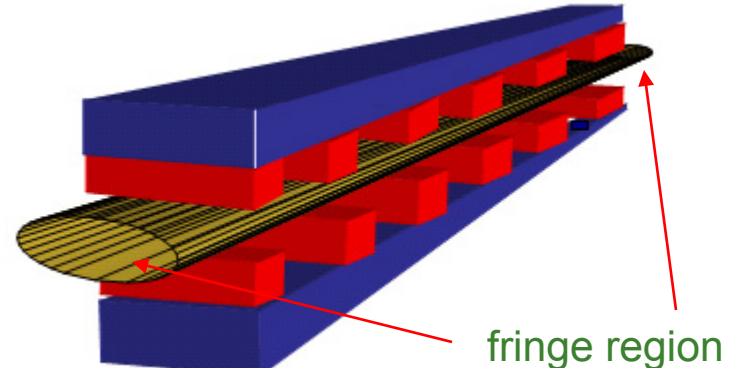
480cm in z, $dz=0.2\text{cm}$

- Field components B_x , B_y , B_z in one quadrant given to a precision of 0.05G.

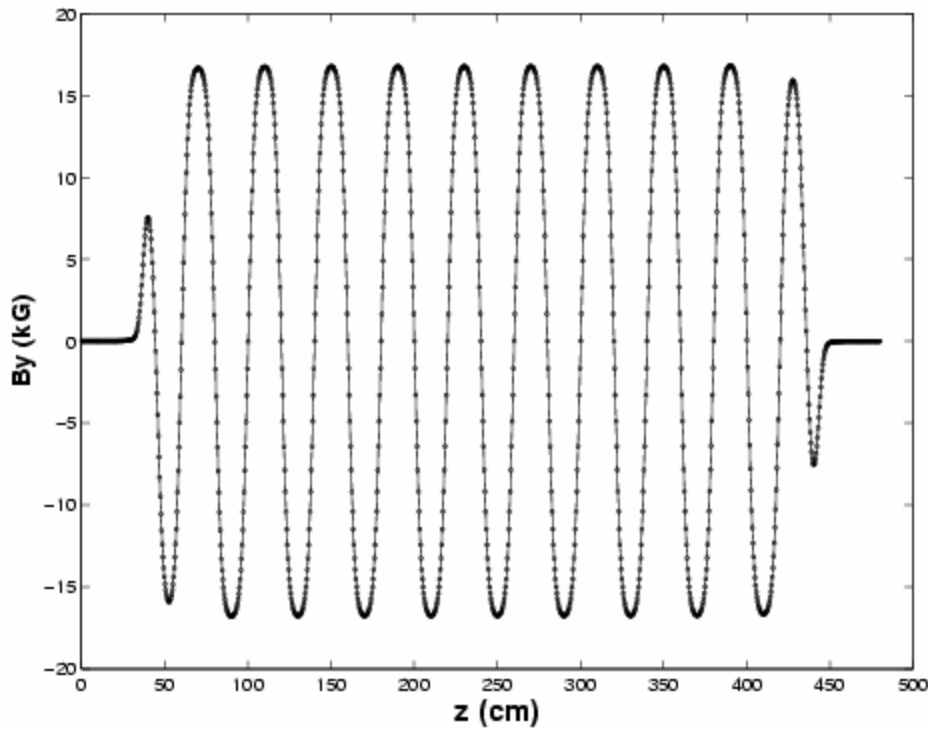
- Place an imaginary elliptic cylinder between pole faces, extending beyond the ends of the magnet far enough that the field at the ends is effectively zero.

- Fit data onto elliptic cylindrical surface using bicubic interpolation to obtain the normal component on the surface.

- Compute the interior vector potential and all its desired derivatives from surface data.

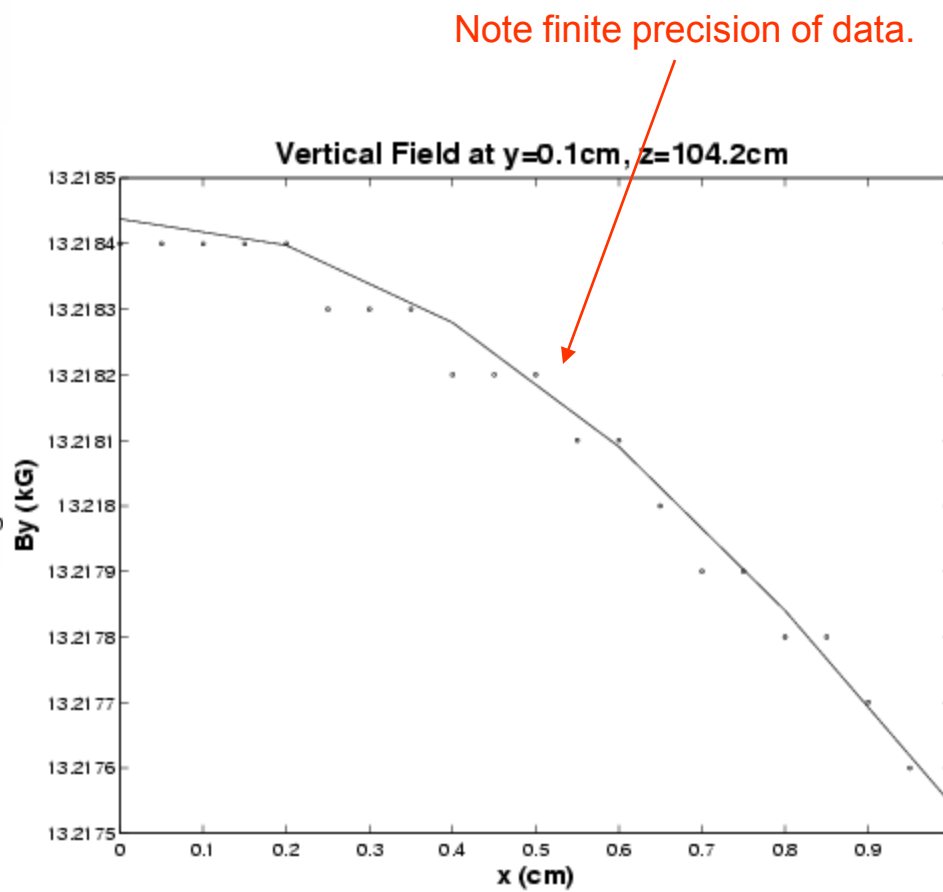


Fit to the Proposed ILC Wiggler Field Using Elliptical Cylinder



Fit to vertical field B_y
at $x=0.4$ cm, $y=0.2$ cm.

Residuals ~ 0.5 G / 17 kG

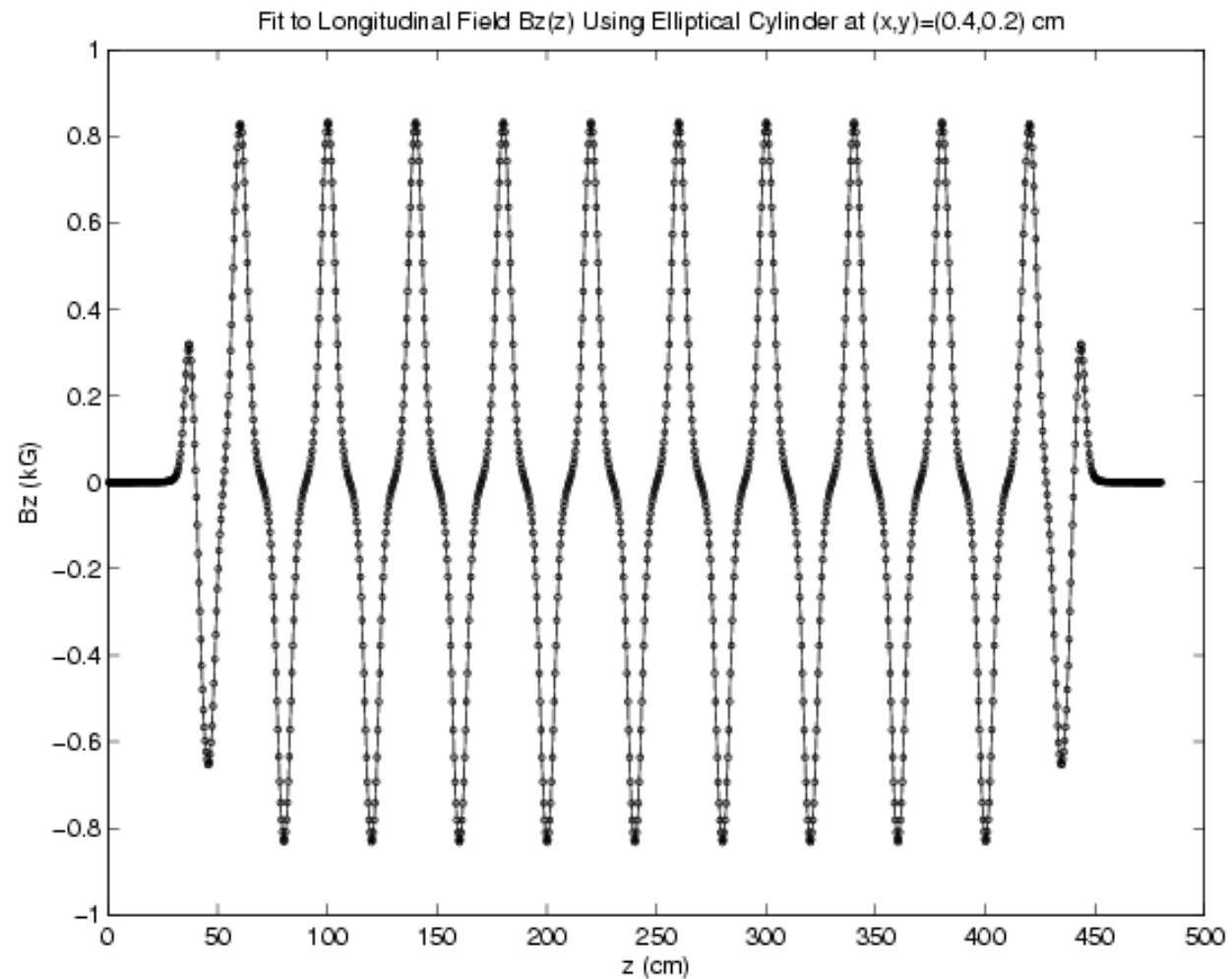


Note finite precision of data.

Fit to the Proposed ILC Wiggler Field Using Elliptical Cylinder

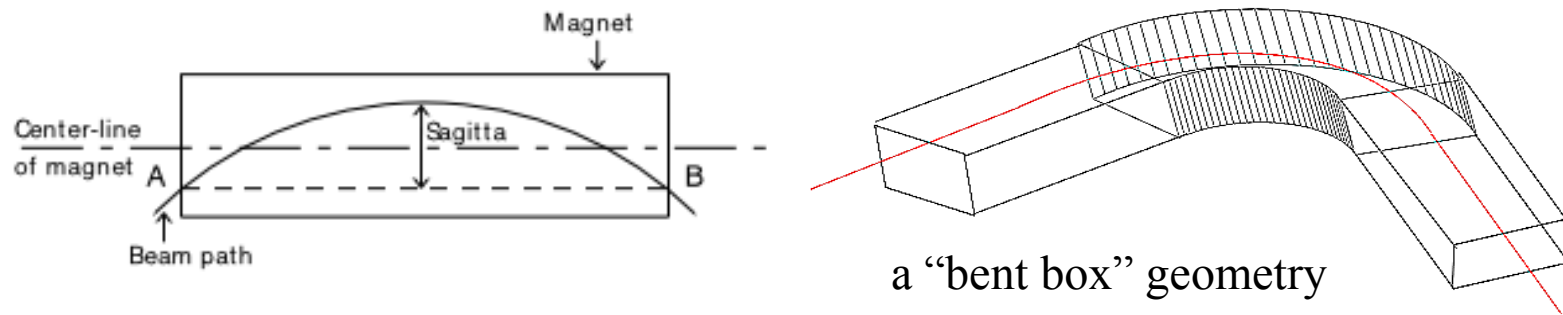
No information
about B_z was
used to create
this plot.

Fit to longitudinal
field B_z at
 $x=0.4\text{cm}$,
 $y=0.2\text{cm}$.



The Bent Box and Other Geometries

- For the straight-axis cylinder domains, only the normal component of \mathbf{B} on the surface is needed to determine the interior vector potential.
- The circular, elliptical, and rectangular cylinder are special in that Laplace's equation is separable for these domains. This is not always possible.
- Surface data for general domains can again be used to fit interior data provided *both* \mathbf{B}_{normal} and ψ are available on the surface. The magnetic vector potential in the interior can be determined by the integration of surface data against a *geometry-independent* kernel.



General Surfaces

Using the Helmholtz theorem and results relating to Dirac monopoles, we may write the interior vector potential in terms of surface data in the form

$$\mathbf{A} = \mathbf{A}^n + \mathbf{A}^t \quad , \text{ where}$$

$$\mathbf{A}^n(\mathbf{r}) = \int_S [\mathbf{n}(\mathbf{r}') \cdot \mathbf{B}(\mathbf{r}')] \mathbf{G}^n(\mathbf{r}; \mathbf{r}', \mathbf{m}(\mathbf{r}')) dS'$$

$$\mathbf{A}^t(\mathbf{r}) = \int_S \psi(\mathbf{r}') \mathbf{G}^t(\mathbf{r}; \mathbf{r}') dS' .$$

The kernels are given by:

$$\mathbf{G}^n(\mathbf{r}; \mathbf{r}', \mathbf{m}) = \frac{\mathbf{m} \times (\mathbf{r} - \mathbf{r}')}{4\pi |\mathbf{r} - \mathbf{r}'| [|\mathbf{r} - \mathbf{r}'| - \mathbf{m} \cdot (\mathbf{r} - \mathbf{r}')]}$$

$$\mathbf{G}^t(\mathbf{r}; \mathbf{r}') = \frac{\mathbf{n}(\mathbf{r}') \times (\mathbf{r} - \mathbf{r}')}{4\pi |\mathbf{r} - \mathbf{r}'|^3}$$

normal component

tangential components

where \mathbf{m} is a unit vector pointing along some line that does not intersect the interior (a Dirac string), and \mathbf{n} is the unit normal to the surface at \mathbf{r}' .

The kernels \mathbf{G}^n and \mathbf{G}^t satisfy the properties:

- Each is analytic in the variables \mathbf{r} at all points in the interior.
- $\nabla \times (\nabla \times \mathbf{G}^t(\mathbf{r}; \mathbf{r}')) = \nabla \times (\nabla \times \mathbf{G}^n(\mathbf{r}; \mathbf{r}', \mathbf{m})) = 0$ for all points \mathbf{r} in the interior.
- $\nabla \cdot \mathbf{G}^t(\mathbf{r}; \mathbf{r}') = \nabla \cdot \mathbf{G}^n(\mathbf{r}; \mathbf{r}', \mathbf{m}) = 0$ for all points \mathbf{r} in the interior.

As a result, the vector potential \mathbf{A} is guaranteed to satisfy Maxwell's equations $\nabla \times (\nabla \times \mathbf{A}) = \nabla \times \mathbf{B} = 0$ and the Coulomb gauge condition $\nabla \cdot \mathbf{A} = 0$.

Given a point along the design orbit, we may construct a power series for \mathbf{A} about \mathbf{r}_d by integrating the surface data against the power series for the \mathbf{G} 's, term-by-term.

Each Taylor coefficient is obtained from a single surface integration.

This has been implemented numerically to compute coefficients a_l^w of the vector potential about any point on the design orbit.

Code accepts as input 3d data of the form (\mathbf{B}, ψ) on a mesh and will produce as output:

- 1) Vector potential \mathbf{A} at any interior point (gauge specified by orientation of strings)
- 2) Taylor coefficients of \mathbf{A} about any design point through degree N

which in turn are used to compute...

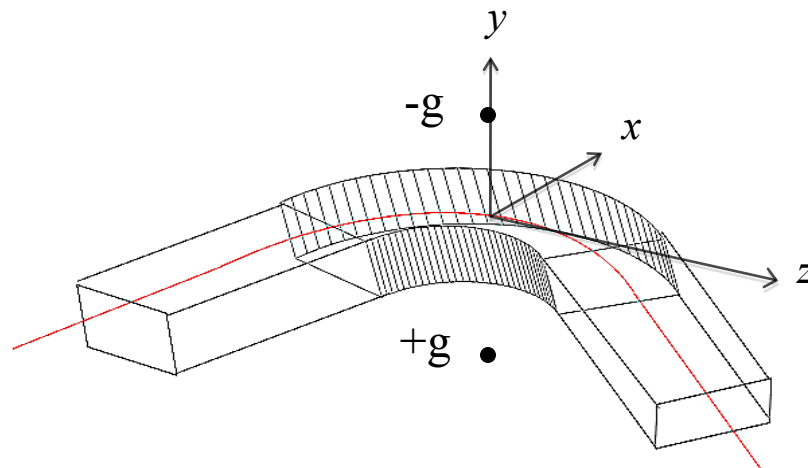
- 3) Interior field \mathbf{B} at any point
- 4) Taylor coefficients of \mathbf{B} about any point
- 5) $\nabla \cdot \mathbf{A}, \quad \nabla \times \mathbf{A}, \quad \nabla \cdot \mathbf{B}, \quad \nabla \times \mathbf{B}$



Code produces interior fits that satisfy Maxwell's equations exactly even if the surface data is noisy and the required surface integrals are performed only approximately.

Transfer maps are then computed from the Taylor expansion of \mathbf{A} along the design orbit.

Monopole Doublet Benchmark

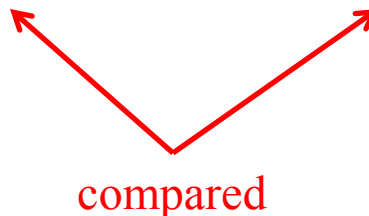


$$g = 1 \text{ T}\cdot\text{cm}^2, a = 2.5 \text{ cm}$$

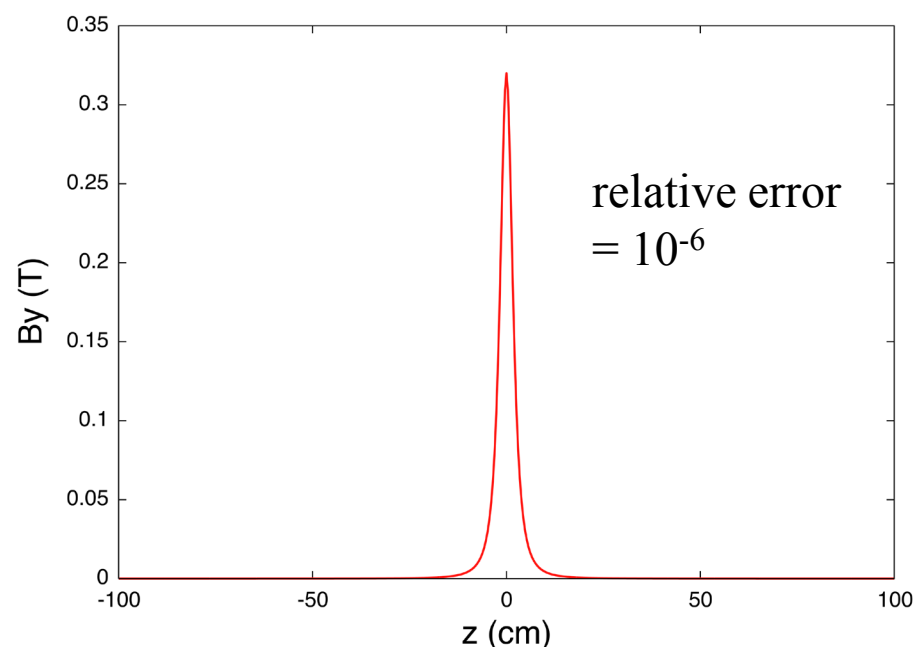
8.65 MeV positrons: 30 degree bend

Exactly soluble, numerically challenging test field.

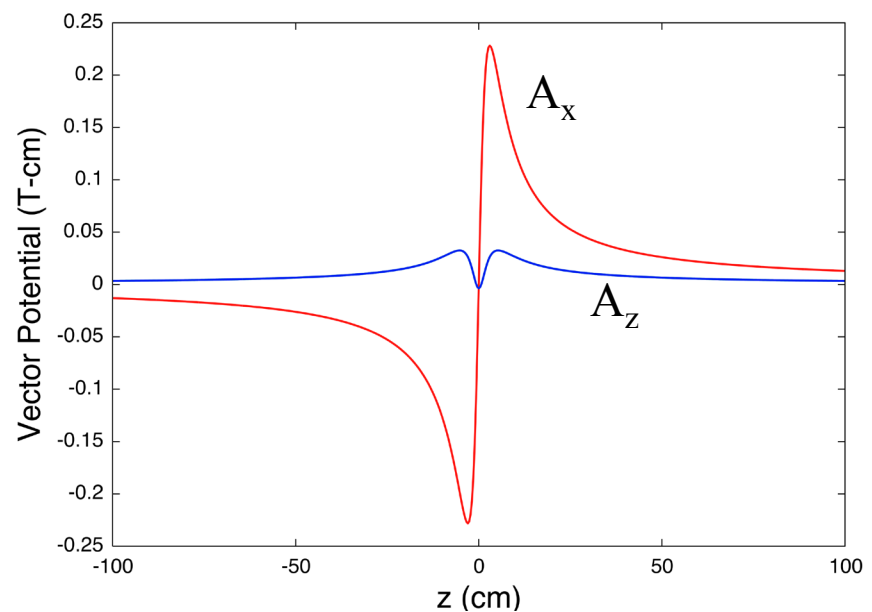
- Magnetic field and its Taylor coefficients are known exactly.
- Vector potential and its Taylor coefficients are known exactly in one gauge.
- Integrate to obtain the reference trajectory and the map about the reference trajectory using 1) exact vector potential, 2) vector potential computed from surface data.

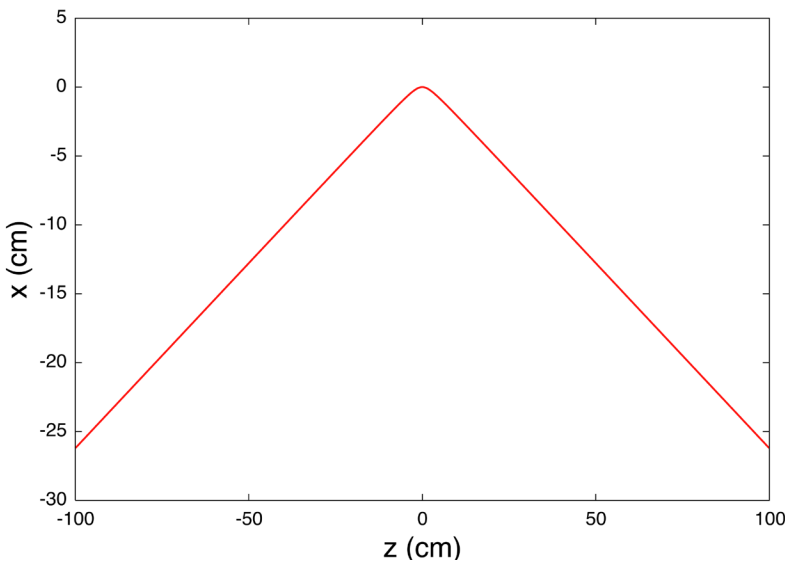


Computed magnetic field

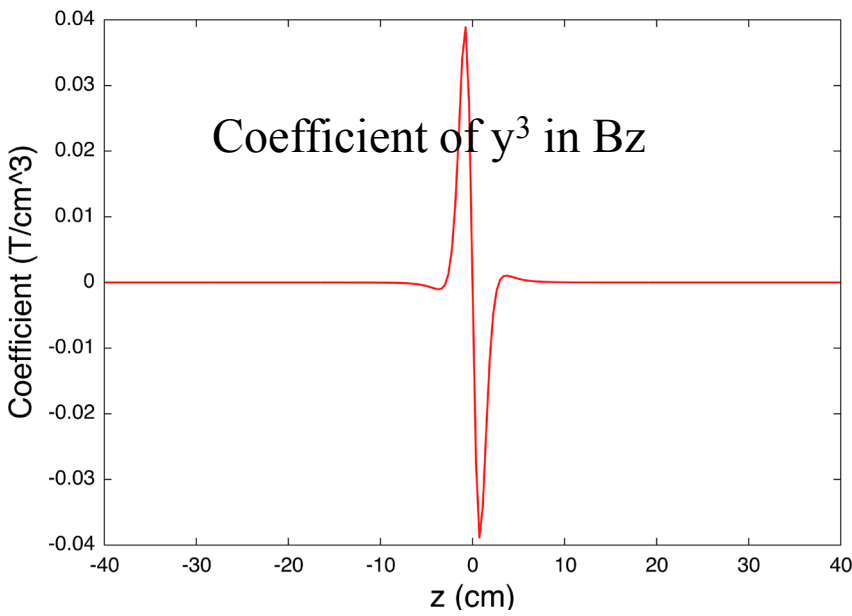


Computed vector potential

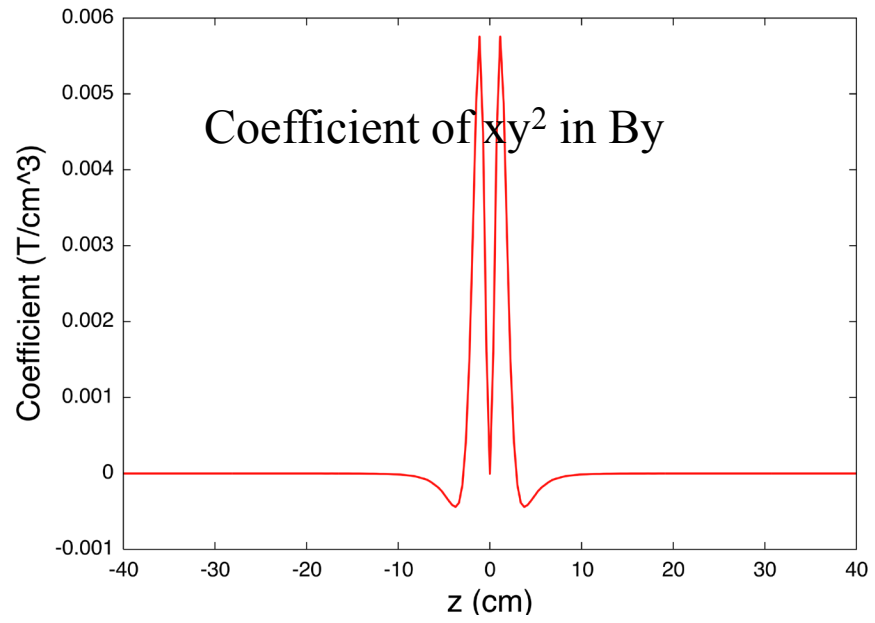




Reference trajectory
largest error in x ,
relative to peak excursion,
is 5×10^{-7}



Field coefficients
worst error/peak $\sim 10^{-4}$
typical error $< 10^{-5}$

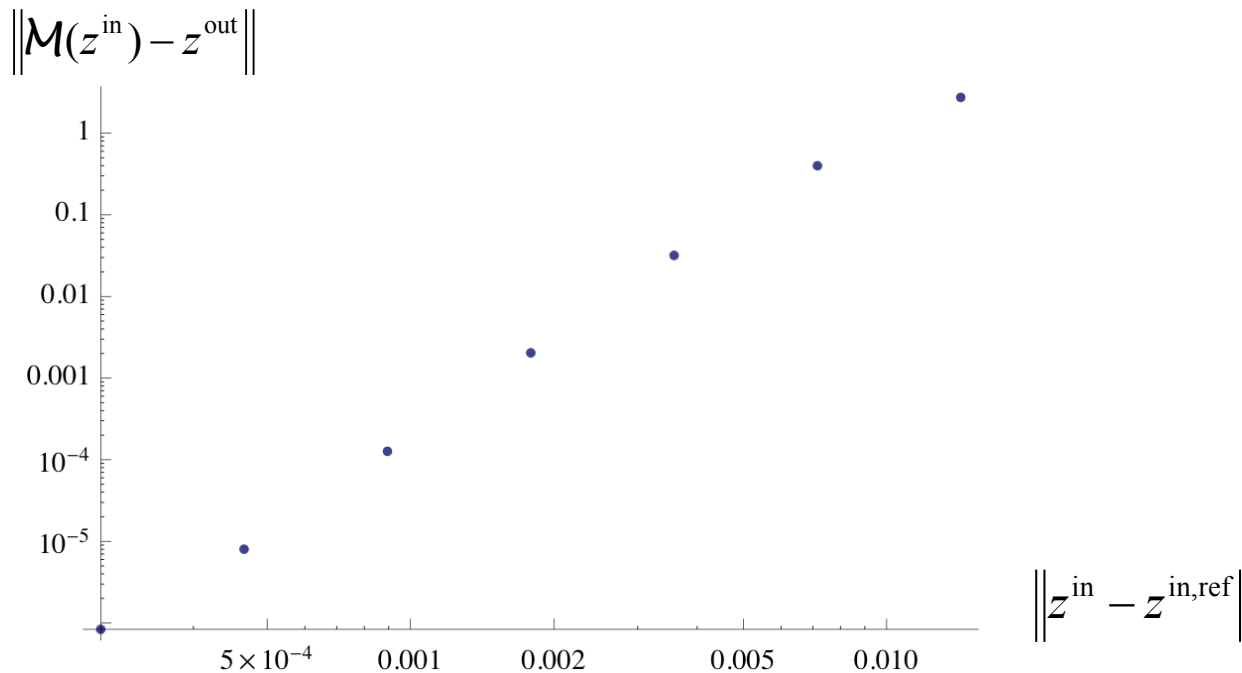


Comparison of Maps

Largest error in linear map and nonlinear generators through f_4 : $\sim 10^{-4}$

Error scales as Δ^4 for trajectories near the reference trajectory, as expected,

where $\Delta = \|z^{\text{in}} - z^{\text{in,ref}}\|$.



Fitting NSLS-II Dipole Data Using a Bent Box

Data provided for the 35-mm gap Brookhaven dipole on the domain:

x in $[-0.06, 0.06]$ m,

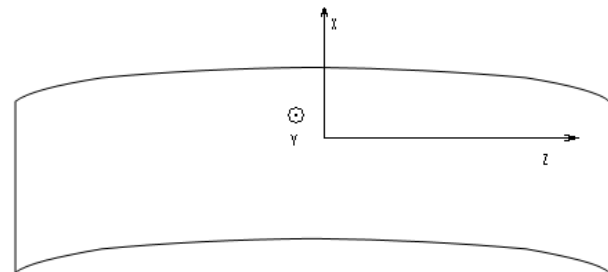
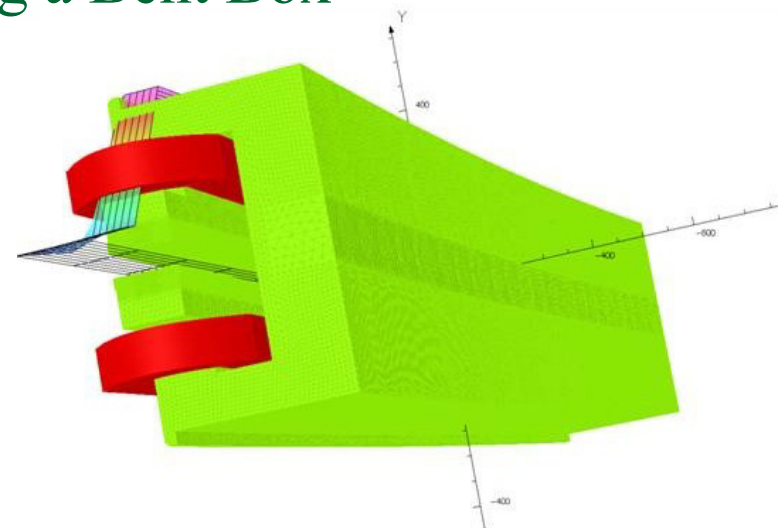
y in $[-0.016, 0.016]$ m,

z in $[-1.8, 1.8]$ m,

Spacing of mesh points $h = 2$ mm

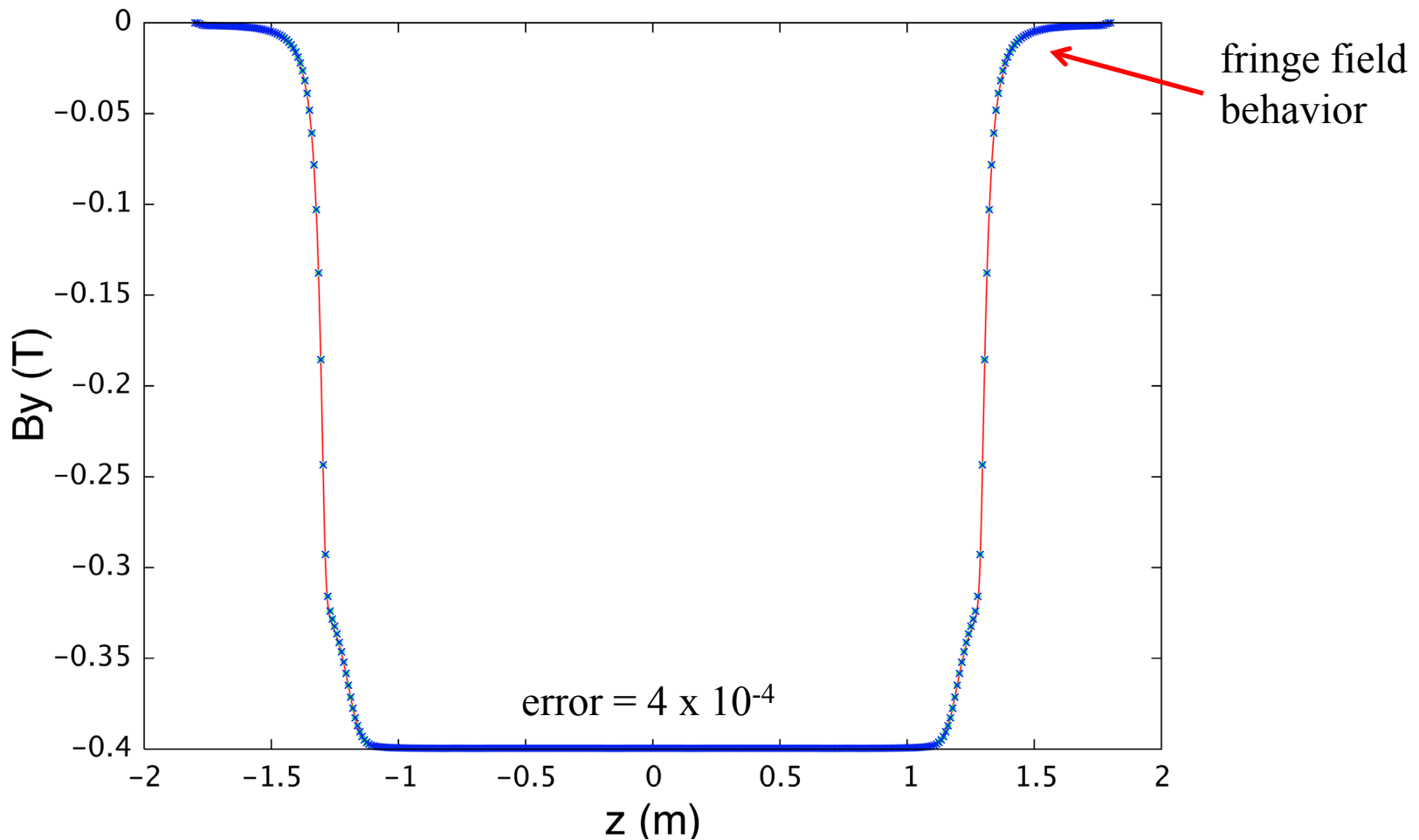
The interior magnetic field was obtained and compared against the numerically computed values provided at the interior mesh points.

The three components of vector potential and their Taylor coefficients were computed through 4th degree to obtain a design orbit and the 3rd order transfer map about that orbit.



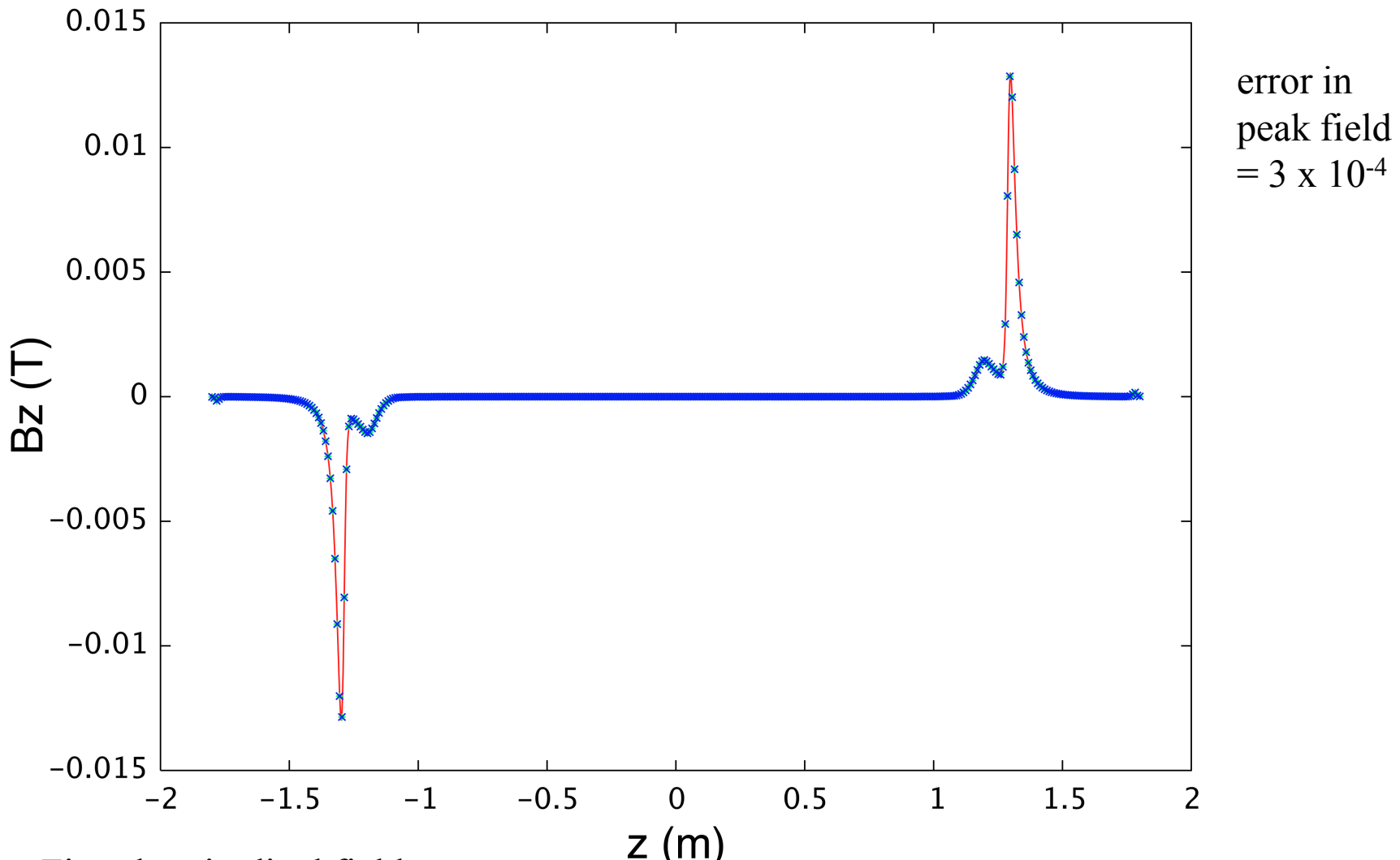
3 GeV electrons: 6 degree bend

Fit to the NSLS-II Dipole Field Using a Bent Box



Fit to vertical field B_y
at $x=0$ cm, $y=0.2$ cm.

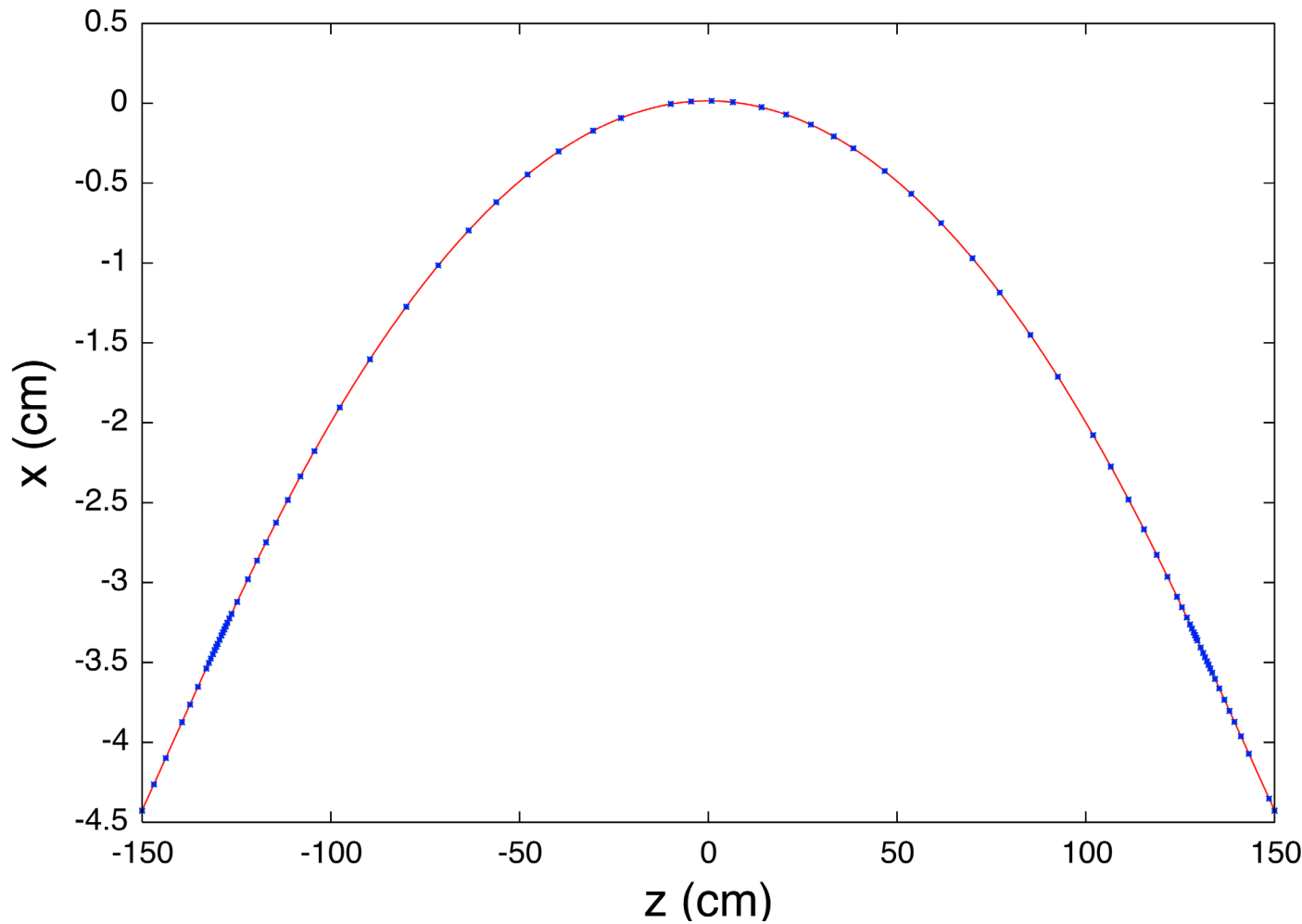
Fit to the NSLS-II Dipole Field Using a Bent Box



Fit to longitudinal field
 B_z at $x=0$ cm, $y=0.2$ cm.

error in
peak field
 $= 3 \times 10^{-4}$

Fit to the NSLS-II Dipole Field Using a Bent Box



Reference trajectory

Conclusions

- Routines have been developed for computing accurate maps for realistic general beamline elements by fitting field data onto boundary surfaces of various geometries.
- An analytic representation of the interior field and all its derivatives is obtained that can be used to compute canonical (using \mathbf{A}) or noncanonical (using \mathbf{B}) maps.
- These techniques have many advantages over on-axis or midplane fitting, including the smoothing of numerical noise present in the original data.
- Error bounds and numerical benchmarks have been investigated in detail.
- These methods have been applied to compute maps for the prototype wiggler of the ILC damping rings and the Brookhaven (NSLS-II) dipoles.

References

- C. Mitchell and A. Dragt, Phys. Rev. ST Accel. Beams 13, 064001 (2010).
- D. Abell, Phys. Rev. ST Accel. Beams 9, 052001 (2006).
- M. Venturini and A. Dragt, Nucl. Inst. and Meth. A 427, 387 (1999).
- A. Dragt, *Lie Methods for Nonlinear Dynamics with Applications to Accelerator Physics*, University of Maryland Technical Report (2011),
<http://www.physics.umd.edu/dsat>.
- C. Mitchell, Ph. D. Thesis, University of Maryland, College Park (2007),
<http://www.physics.umd.edu/dsat>.